Chemical Physics 381 (2011) 11–20

Contents lists available at ScienceDirect

Chemical Physics

journal homepage: www.elsevier.com/locate/chemphys

Vibrational and thermodynamic properties and molecular motions in the incommensurate crystal of morpholinium tetrafluoroborate studied by ^{1}H NMR

M. Owczarek [a], R. Jakubas [a,*], G. Bator [a], A. Pawlukojć [b], J. Baran [c], J. Przesławski [d], W. Medycki [e]

[a] Faculty of Chemistry, University of Wrocław, F. Joliot-Curie 14, 50-383 Wrocław, Poland
[b] Institute of Nuclear Chemistry and Technology, Dorodna 16, 03-195 Warsaw, Poland
[c] Institute of Low Temperature and Structural Research of the PAS, Okòlna 2, 50-422 Wrocław, Poland
[d] Institute of Experimental Physics, University of Wrocław, Max Born Sq. 9, 50-204 Wrocław, Poland
[e] Institute of Molecular Physics, PAS, Smoluchowskiego 17, 60-179 Poznań, Poland

ARTICLE INFO

Article history:
Received 23 August 2010
In final form 5 January 2011
Available online 9 January 2011

Keywords:
AC calorimetry
^{1}H NMR
Infrared
DFT calculation
Morpholinium tetrafluoroborate

ABSTRACT

Dynamics of molecules in morpholinium tetrafluoroborate, $[NH_2(C_2H_4)_2O][BF_4]$, has been studied in a wide temperature range by means of AC calorimetry, ^{1}H NMR and infrared spectroscopy. Simultaneously, DFT (density functional theory) calculations of the molecular structure and normal vibration frequencies have been performed by using various functionals for initial structural data of the low temperature phase. Infrared spectra of polycrystalline $[NH_2(C_2H_4)_2O][BF_4]$ have been analyzed in a frequency range 4000–400 cm^{-1}. Substantial changes in a temperature evolution of internal modes of both morpholinium cations and $[BF_4]^-$ anions are due to the freezing of these moieties motions below 117 K. A dynamic non-equivalence of protons involved in N–H···F and N–H···O hydrogen bonds has been detected. Heat capacity anomalies around structural phase transitions detected by AC calorimetry (117 and 153 K) have been evaluated and described. A molecular mechanism of the phase transitions is discussed on the basis of presented results.

1. Introduction

Investigations of compounds built up of organic cations and either inorganic or organic anions are of value as they provide interesting supramolecular networks. The characteristic feature of these networks is that the moieties can participate in hydrogen bond systems. Hydrogen bonds have been recognized as the most powerful force to generate supramolecular assemblies of molecules. In such systems we can combine desirable properties of inorganic materials with high non-linear optical activity of organic substances [1–5]. The most interesting feature in these connections is the presence of non-linear optical activity (NLO) and ferroelectric properties. In the case of morpholinium connections with inorganic moieties the NLO effect was found in e.g. morpholinium dihydrogenphosphate [6]. Numerous quite simple (1 : 1) ionic connections of morpholinium cations with organic acid anions [7,8], mainly with substituted benzoic acid (e.g. 4-hydroxybenzoic, 2-chloro-4-nitrobenzoic and 2,3-dicyanohydroquinone [9–11]), are also characterized by NLO properties at room temperature. Recently, the first series of thermotropic ionic liquid crystals based on the morpholinium core has been reported [12]. Several examples of simple ionic morpholinium (M) complexes with tetrahedral AB_4-type anions: $MHSO_4$ [13], $MClO_4$ [14] and $MReO_4$ [15] were synthesized. They are closely related to the compound under investigation, $[NH_2(C_2H_4)_2O][BF_4]$, taking into account their polymeric organic network.

The previous calorimetric (DSC) measurements of $[NH_2(C_2H_4)_2O][BF_4]$ disclosed quite a complex sequence of phase transitions (PTs) at low temperature [16]:

$$\underset{\mathbf{III}}{P2_12_12_1} \;\overset{117/119\ \mathrm{K}}{|}\; \underset{\mathbf{II}}{modulated} \;\overset{153\ \mathrm{K}}{|}\; \underset{\mathbf{I}}{Pnam} \longrightarrow T[K]$$

The phase transition (PT) **I** → **II** appears continuous, whereas the low temperature one, **II** → **III**, exhibits discontinuous character. The latter PT is accompanied by a significant transition entropy value, which is explained in terms of an order–disorder mechanism. Single crystal X-ray diffraction studies showed that the disordered high temperature orthorhombic phase **I** and the low temperature ordered orthorhombic phase **III** are separated by a narrow intermediate phase **II**, which appeared to be modulated incommensurably [16,17]. The **II** → **III** phase transition is accompanied by a tripling of the unit cell volume ($c_{III} = 3c_I$). This phase transition is classified as a nonferroelectric one. Nevertheless, such a sequence

* Corresponding author. Fax: +48 713282348.
E-mail address: rj@wchuwr.chem.uni.wroc.pl (R. Jakubas).

0301-0104/$ - see front matter © 2011 Elsevier B.V. All rights reserved.
doi:10.1016/j.chemphys.2011.01.002

of phase transitions is typical of ferroelectric materials with a "lock-in" discontinuous transition [18,19]. The crystal structure of $[NH_2(C_2H_4)_2O][BF_4]$ in the phase **I** consists of morpholinium cations, forming one-dimensional hydrogen-bond network, and highly disordered tetrafluoroborate anions (see Fig. 1). The dynamics of anionic moieties was suggested to contribute to the **II** → **III** PT mechanism. The role of morpholinium cations in the mechanism of both transitions is unclear. Nevertheless, the isotopic effect is visible as a shift of temperature of both phase transitions by about 7 K. It means that N–H···F and N–H···O hydrogen bonds may be involved in the dynamics of molecules in the crystal structure. In order to throw more light on the molecular mechanism of the phase transitions we decided to carry out precise AC calorimetric measurements, vibrational and proton magnetic resonance (^{1}H NMR) studies in a wide temperature range on the $[NH_2(C_2H_4)_2O][BF_4]$ crystal.

2. Experimental

Colorless and transparent single crystals of $[NH_2(C_2H_4)_2O][BF_4]$ were obtained by a stoichiometric reaction (1 : 1) of morpholine and fluoroboric acid. The chemical formula of the compound was confirmed by an elemental analysis (found: C, 26.56%; N, 7.69%; H, 5.47%; calculated: C, 26.67%; N, 7.78%; H, 5.56%). The obtained crystals were twice recrystallized from a methanol solution. Single crystals were grown by slow evaporation of the solution at constant room temperature (RT). A deuterated compound $[ND_2(C_2H_4)_2O][BF_4]$ was obtained by dissolution of $[NH_2(C_2H_4)_2O][BF_4]$ crystals in D_2O and evaporation in vacuum conditions. The material was twice recrystallized from D_2O.

Infrared spectra of $[NH_2(C_2H_4)_2O][BF_4]$ were measured in a wide temperature range (at cooling runs) for mulls in Nujol and Fluorolube (only RT) with a Bruker IFS-88 spectrometer over the wavenumber range 4000–500 cm^{-1} with a resolution of 1 cm^{-1}. APD Cryogenics with closed cycle helium cryodyne system was used for temperature-dependent studies. The temperature of the sample was maintained at the accuracy of 0.1 K. Powder FT-Raman spectra were measured with a FRA-106 attachment to the Bruker IFS-88 spectrometer over the wavenumber range 3500–80 cm^{-1} at room temperature. Grams/368 Galactic Industries program was used for numerical fitting of the experimental data. Gaussian functions were used for fitting the infrared bands.

A computer controlled AC calorimeter (Sinku-Riko ACC-1 M/L) has been used. Thermal response was detected by a chromel-constantan thermocouple using a lock-in amplifier. The AC calorimetric measurements were performed with a chopping frequency of 0.8 Hz during heating and cooling at the rate of 0.05 K/min.

T_1 (^{1}tH NMR) relaxation time measurements were performed on a ELLAB TEL-Atomic PS 15 spectrometer working at the frequency of 25 MHz. The temperature of the sample was automatically stabilized by a UNIPAN 650 temperature controller operating with a Pt-100 sensor. The T_1 relaxation times were determined by using a saturation method. The powdered sample of the crystal was degassed under pressure of 10^{-5} Torr (1.32×10^{-3} bar) and sealed under vacuum in glass ampoules.

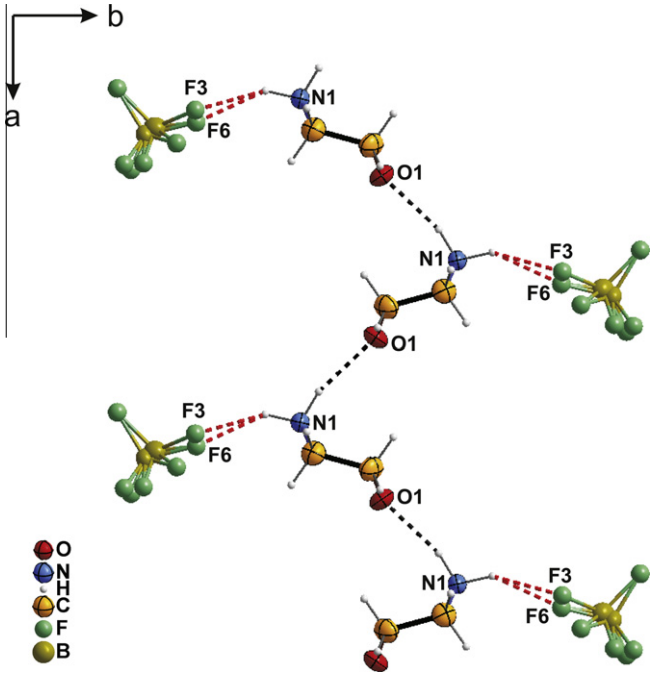

Fig. 1. Hydrogen bonds network in $[NH_2(C_2H_4)_2O][BF_4]$ (phase **I**).

3. Structural data

We have theoretically calculated molecular geometries and IR frequencies for the isolated $[BF_4]^-$ anion and the morpholinium cation as well as for a solid state model of the $[NH_2(C_2H_4)_2O][BF_4]$ salt. We have used DMol3 program [20,21] from Materials Studio package [22] for the Becke–Lee–Yang–Parr correlation functional (BLYP) [23,24] and dnp (double numerical and polarization on heavy and hydrogen atoms) basis sets as implemented in DMol3. An initial data set for the calculations was taken from crystallographic data (80 K). For the system of two hundred and fifty-two (252) atoms in the crystallographic unit cell seven hundred and fifty-three (753) frequency modes have been obtained in which six hundred and twelve (612) describe normal vibrations of twelve (12) $[BF_4]^-$ anions and of twelve (12) morpholinium cations, and one hundred and forty-one (141) describe translational and rotational modes of twelve anion-cation pairs of the $[NH_2(C_2H_4)_2O][BF_4]$ salt in the phase **III**. The corresponding modes of morpholinium tetrafluoroborate were defined by means of internal coordinates according to [25]. Theoretically predicted frequencies were not scaled.

A comparison of experimental bond lengths and angles with the calculated ones in the crystalline phase (80 K) as well as for the isolated molecule is presented in Table 1. From these data, it clearly follows that the tetrahedral geometry of anions is somewhat different from that calculated for the crystal. B–F distances differ by *ca.* 0.03 Å. The geometry of $[NH_2(C_2H_4)_2O]^+$ cations obtained from X-ray measurements is slightly distorted. C–C and C–N bond lengths are in good agreement with the calculated data for the crystal. The most visible change is seen in C–O bond length which is almost the same as for isolated molecules. The average difference in torsion angles is ±1.5° (max. ~5° for C–C–O–C) which can be a consequence of a formation of N–H···O and N–H···F hydrogen bonds.

4. Selection rules

In the high temperature phase the crystal is orthorhombic and belongs to the *Pnam* space group. The unit cell contains four formal molecules ($Z = 4$). Taking into account only these data, both cations and anions should occupy $C_s(xy)$ sites. The C_s site symmetry of the morpholinium cations follows from the X-ray data. The following atoms: N1, O1, H1C and H1D occupy the *m* symmetry plane being parallel to the *ab*(*xy*) crystallographic plane. Internal modes of this cation may be classified as A′(23) and A″(19). Due to the correlation field (Davydov) splitting each internal mode splits into four ($A' \rightarrow A_g+B_{1g}+B_{2u}+B_{3u}$; $A'' \rightarrow B_{2g}+B_{3g}+A_u+B_{1u}$) unit cell modes (see Table 2).

Table 1
Calculated structure (distances in Å and angles in °) of the isolated molecule, in the crystal and from X-ray single crystal diffractional studies of $[NH_2(C_2H_4)_2O][BF_4]$.

Coordinates	Calculated DMol3 (BLYP/dnp)		Observed
	Isolated molecules	Crystal	80 K
B–F	1.434	1.428, 1.420, 1.428	1.397, 1.393, 1.399
		1.431, 1.417, 1.429	1.400, 1.392, 1.392
		1.417, 1.421, 1.416	1.395, 1.394, 1.393
		1.423, 1.441, 1.423	1.396, 1.410, 1.396
F–B–F	109.47	109.81, 111.11, 109.84	110.37, 111.11, 110.60
		109.49, 109.81, 109.78	109.32, 109.46, 109.86
		110.40, 109.45, 110.29	110.30, 109.69, 110.21
		109.43, 108.47, 108.09	109.00, 108.14, 108.03
O–C	1.435	1.452, 1.460	1.434, 1.444
		1.455, 1.453	1.435, 1.432
		1.459, 1.452	1.440, 1.435
C–C	1.530	1.524, 1.519	1.516, 1.517
		1.519, 1.525	1.514, 1.516
		1.519, 1.523	1.515, 1.515
N–C	1.540	1.509, 1.513	1.499, 1.496
		1.509, 1.512	1.496, 1.501
		1.512, 1.509	1.500, 1.495
O–C–C	110.81	110.75, 109.74, 110.19	111.08, 110.10, 110.34
	110.78	110.05, 110.48, 110.66	110.22, 110.66, 110.59
C–C–N	108.61	109.21, 109.31, 109.84	108.65, 109.05, 109.12
	108.7	109.29, 109.69, 108.95	109.29, 109.38, 108.82
C–N–C	112.14	111.12, 111.27, 111.06	110.43, 110.45, 110.09
C–O–C	111.63	111.17, 110.82, 111.25	110.75, 110.50, 110.90
O–C–C–N	−56.36	−56.90, −56.11, −57.48	−58.22, −57.26, −58.07
C–C–N–C	52.12	55.17, 53.80, 56.15	56.30, 54.94, 57.02
C–N–C–C	−52.17	−56.03, −55.27, −55.79	−56.74, −55.96, −57.07
N–C–C–O	56.51	57.95, 58.86, 57.49	58.12, 59.27, 58.66
C–C–O–C	−63.51	−61.08, −67.67, −60.75	−60.55, −62.45, −60.89
C–O–C–C	63.4	60.65, 61.34, 60.60	61.00, 61.49, 60.49

Assuming that the tetrafluoroborate anions occupy the C_s sites one expects the following correlation for its internal modes: $\nu_1(A_1) \rightarrow A'$; $\nu_2(E) \rightarrow A'+A''$; $\nu_3(F_2) \rightarrow 2A'+A''$; $\nu_4(F_2) \rightarrow 2A'+A''$. Additionally, each component of the internal modes splits into four unit cell modes (see above). The expected splitting are given in Table 2. However, the X-ray data suggest a disorder for these anions. It is suggested that only F1 atoms occupy the C_s site. In such a case, the real local symmetry for tetrafluoroborate anions will be C_1 and the correlation (unit cell or Davydov) type splitting cannot occur. In this case, it is impossible to perform the formal classification of the unit cell modes either.

In the low temperature phase **III** the title crystal belongs to the $P2_12_12_1(D_2^4)$ space group of the orthorhombic system. The unit cell contains 12 formal molecules, the asymmetric unit consists, however, of three ($Z' = 3$) formal molecules; i.e. three $[BF_4]^-$ tetrahedral anions and three morpholinium cations. Each of them occupies the general $C_1(4)$ sites. For each formal molecule (i.e. for each anion and each cation) its normal modes split into four unit cell modes ($A + B_1 + B_2 + B_3$). In this approach, the dynamical coupling between the normal modes of various components of the asymmetric unit are negligible. The results of the formal fundamental modes ($k = 0$) are given in Table 3.

5. IR and Raman spectra

Infrared spectra of polycrystalline $[NH_2(C_2H_4)_2O][BF_4]$ in a wavenumber range between 4000 and 500 cm^{-1} at 10, 80 (phase **III**) and 300 K (phase **I**) and Raman spectra (300 K) are presented

Table 2
The formal classification of the fundamental modes (k = 0) for the $[NH_2(C_2H_4)_2O][BF_4]$ crystal in the phase **I** (space group *Pnam* Z = 4). It is assumed that both ions occupy the $C_s(xy)$ sites. According to the X-ray data, $[BF_4]^-$ anions occupy the C_1 sites. In such a case, the classification of $[BF_4]^-$ modes is not possible.

Site[a]	UCG	Lattice modes			Internal modes					Selection rules[b]	
					$[NH_2(C_2H_4)_2O]^+$	$[BF_4]^-$					
$C_s(xy)$	D_{2h}	Ac	Lib	Tran		$\nu_1(A_1)$ 769[c]	$\nu_2(E)$ 353	$\nu_3(F_2)$ 1075	$\nu_4(F_2)$ 524	IR	Raman
	A_g	0	2	4	23	1	1	2	2	*i*	*xx*, *yy*, *zz*
	B_{1g}	0	2	4	23	1	1	2	2	*i*	*xy*
$A' \rightarrow$											
	B_{2u}	1	2	3	23	1	1	2	2	*y*	*i*
	B_{3u}	1	2	3	23	1	1	2	2	*z*	*i*
	B_{2g}	0	4	2	19	0	1	1	1	*i*	*zx*
	B_{3g}	0	4	2	19	0	1	1	1	*i*	*yz*
$A'' \rightarrow$											
	A_u	0	4	2	19	0	1	1	1	*i*	*i*
	B_{1u}	1	4	1	19	0	1	1	1	*x*	*i*

[a] *Abbreviations: Site – group of site symmetry; UCG – unit cell group (equivalent to the factor group); Ac – acoustic modes; Lib. – librational lattice modes; Tran – translational lattice modes.*
[b] *i* – inactive modes.
[c] The wavenumbers of the internal modes for the isolated $[BF_4]^-$ anion of the T_d symmetry (according to [26]).

Table 3
The formal classification of the fundamental modes ($k = 0$) for $[NH_2(C_2H_4)_2O][BF_4]$ for the low temperature phase (orthorhombic system, space group $P2_12_12_1$ (D_2^4); $Z = 12$; $Z' = 3$).

Lattice modes[a]				Internal modes[b]					Selection rules	
				$[NH_2(C_2H_4)_2O]^+$	$[BF_4]^-$					
D_2	Ac	Lib	Tran		$\nu_1(A_1)$ 769[c]	$\nu_2(E)$ 353	$\nu_3(F_2)$ 1075	$\nu_4(F_2)$ 524	IR	Raman
A	0	18	18	42 (126)	1 (3)	2 (6)	3 (9)	3 (9)	*i*	*xx*, *yy*, *zz*
B_1	1	18	17	42 (126)	1 (3)	2 (6)	3 (9)	3 (9)	*z*	*xy*
B_2	1	18	17	42 (126)	1 (3)	2 (6)	3 (9)	3 (9)	*y*	*zx*
B_3	1	18	17	42 (126)	1 (3)	2 (6)	3 (9)	3 (9)	*x*	*yz*

[a] *Abbreviations*: Ac – acoustic modes; Lib – librational modes; Tran – translational modes.
[b] Outside of brackets – the number of modes for one molecule in the asymmetric unit; in brackets – the number of modes for asymmetric unit (i.e. for three molecules (ions)).
[c] The wavenumbers of the internal modes for the isolated $[BF_4]^-$ anion of the T_d symmetry (according to [26]).

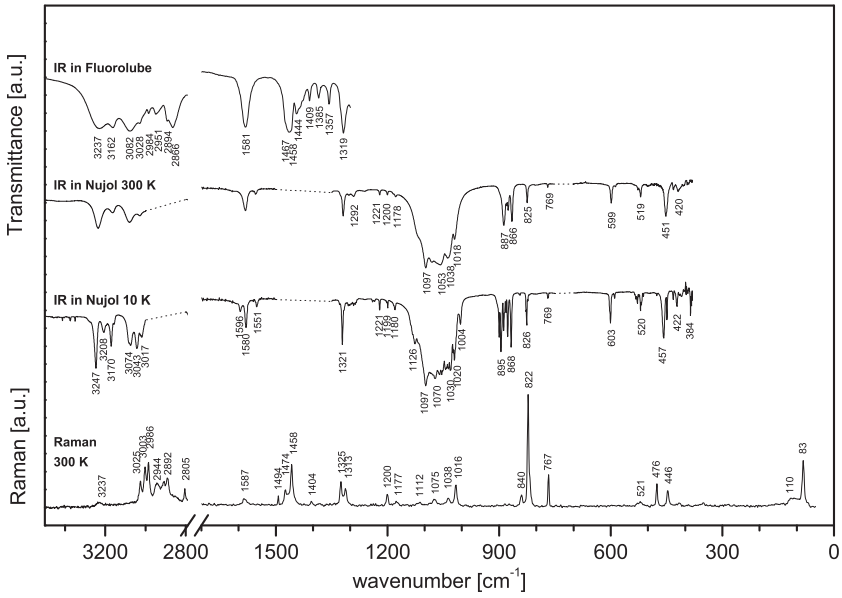

Fig. 2. The infrared spectra of the powdered $[NH_2(C_2H_4)_2O][BF_4]$ sample in Nujol (10 and 300 K) and in Fluorolube (300 K) and the Raman spectrum at 300 K.

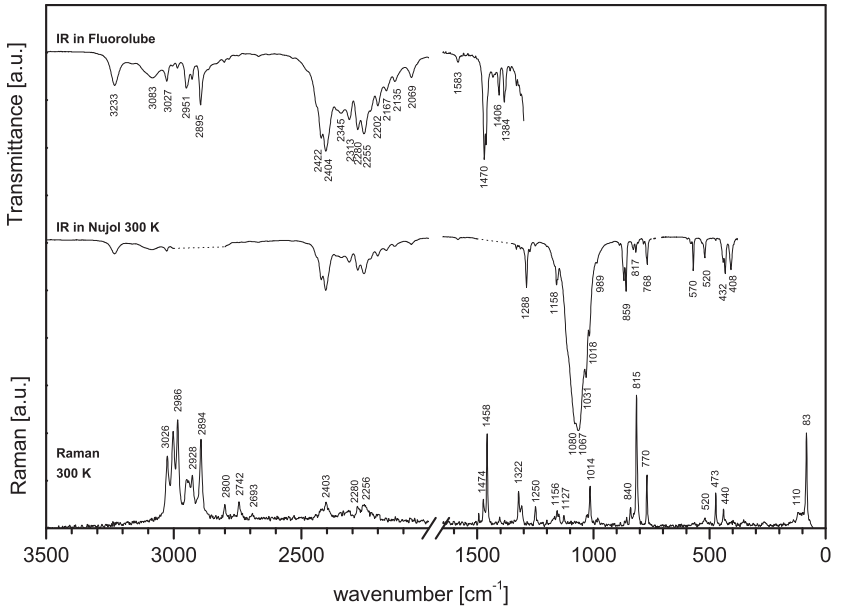

Fig. 3. The infrared spectra of the powdered deuterated $[ND_2(C_2H_4)_2O][BF_4]$ sample in Nujol (10 and 300 K) and in Fluorolube (300 K) and the Raman spectrum at 300 K.

Table 4
Comparison of the selected experimental and calculated IR and Raman spectral data for $[NH_2(C_2H_4)_2O][BF_4]$ and for the deuterated homologue.

Calculated DMol3 (blyp/dnp)		Observed						Tentative assignments
Isolated ions	Crystal	Non-deuterated				Deuterated		
		IR			Raman	IR	Raman	
80 K	80 K	10 K	80 K	300 K	300 K	300 K	300 K	
		3247(s)	3247(m)	3237(m)	3237(vw)	3233(vw)		
		3208(w)	3211(w)					
3380	3306	3170(m)	3169(w)					$\nu(NH_2^+)$
	3301	3156(vw)	3156(sh)	3162(w)				or
	3251	3084(sh)	3081(m)	3082(w)		3083(w)*		N–H···Y
3319	3132	3074(s)	3071(sh)		3071(vw)			(Y = O, F)
	3129	3043(s)	3040(w)		3041(vw)			
	3128							
						2422(w)	2417(vw)	
						2404(w)	2403(vw)	$\nu(ND_2^+)$
						2313(vw)	2310(vw)	or
						2280(vw)	2280(vw)	N–D···Y
						2255(vw)	2256(vw)	(Y = O, F)
						2229(sh)	2227(vw)	
1622	1624	1596(vw)	1594(vw)		1587(vw)			
	1601	1580(w)	1580(m)	1581(w)	1581(sh)	1583(vw)*		$\delta(NH_2^+)$
	1595							
1373	1408			1444*(m)	1444(sh)		1442(vw)	
	1407			1436*(sh)	1433(vw)	1432(w)*	1433(vw)	$\omega(NH_2^+)$
	1399							
1280	1246							
	1242			1357*(m)	1355(vw)	1359(vw)*	1357(vw)	$\tau(NH_2^+)$
	1233							
968	988						1222(vw)	
	981	1221(vw)	1221(w)	1221(vw)	1216(vw)		1217(vw)	ν(C–N)
	966							
						1167(vw)		
						1158(w)	1156(vw)	$\delta(ND_2^+)$
						1153(w)	1148(vw)	
847	900	1126(s)	1126(s)		1120(vw)	1123(sh)	1127(vw)	
	885	1118(sh)	1118(sh)		1117(vw)		1121(sh)	
	882			1109(sh)	1112(vw)		1111(vw)	$\rho(NH_2^+)$
		1097(vs)	1097(vs)	1097(vs)			1096(vw)	
1012	1026		1084(vs)	1084(vs)	1085(vw)			
	1021	1078(sh)	1077(vs)		1075(vw)	1080(vs)	1080(vw)	
	1018	1070(vs)	1071(vs)	1069(sh)	1071(vw)		1072(vw)	
1012	1014					1067(vs)	1065(vw)	
	1010	1061(vs)	1059(vs)				1060(vw)	$\nu_3(BF_4)$
	1007	1052(vs)	1054(vs)	1053(vs)				
1012	1003		1050(sh)					
	999							
	994							
742	795		1045(sh)		1045(vw)			
	792	1043(vs)	1042(vs)				1042(vw)	ν(C–N)
	790							
						986(vw)	987(vw)	$\tau(ND_2^+)$
							980(vw)	
1154	1071	900(m)	900(sh)					
	1063		898(m)					
	1057	895(s)	894(sh)	894(sh)				
1021	1039	893(sh)	893(s)					
	1036	888(sh)	887(s)	887(s)				$\rho(CH_2)$
	1034	885(m)	884(vw)	883(sh)	884(vw)		883(vw)	
1013	1033	882(w)	881(w)	880(sh)				
	1031	877(m)	877(s)	876(m)	873(vw)			
	1027							
963	867	868(s)	867(s)	866(m)		869(w)	865(vw)	
	863							
	859					859(w)	857(vw)	
837	840	844(vw)	844(vw)		840(vw)		840(vw)	ν(C–C)
	837							
	834							
						817(vw)	815(vs)	$\rho(ND_2^+)$
						806(vw)		
707	732					772(vw)		
	730	769(vw)	769(vw)	769(vw)	767(w)	768(vw)	770(w)	$\nu_1(BF_4)$
	729							
479	508	532(vw)	532(vw)				533(vw)	
	506	528(vw)	528(vw)	527(vw)	528(vw)		527(vw)	

(*continued on next page*)

Table 4 (*continued*)

Calculated DMol3 (blyp/dnp)		Observed						Tentative assignments
Isolated ions	Crystal	Non-deuterated				Deuterated		
		IR			Raman	IR	Raman	
80 K	80 K	10 K	80 K	300 K	300 K	300 K	300 K	
	502		524(vw)					
479	498	520(w)	520(w)		521(vw)	520(vw)	520(vw)	
	494	518(sh)	518(sh)	519(vw)	517(sh)			$\nu_4(BF_4)$
	491	512(vw)	513(vw)		513(vw)		513(vw)	
479	489							
	487							
	486							

vs, very strong; s, strong; m, medium; w, weak; vw, very weak; sh, shoulder; ∗ in Fluorolube ν – stretching; δ – scissoring; ρ – rocking; τ – twisting; ω – wagging.

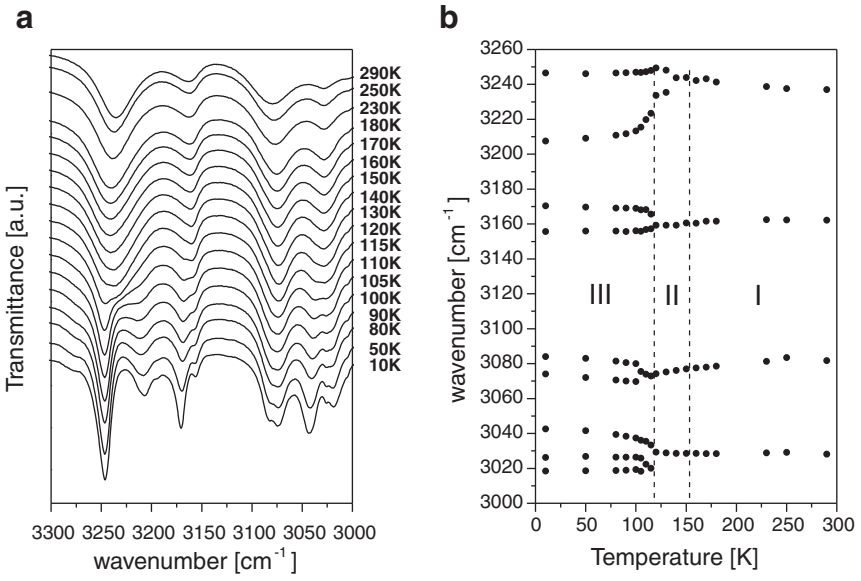

Fig. 4. (a) Temperature evolution of the IR spectra in the $\nu(NH_2^+)$ vibration region (3300–3000 cm^{-1}) and (b) the wavenumber positions of these modes between 10 and 300 K.

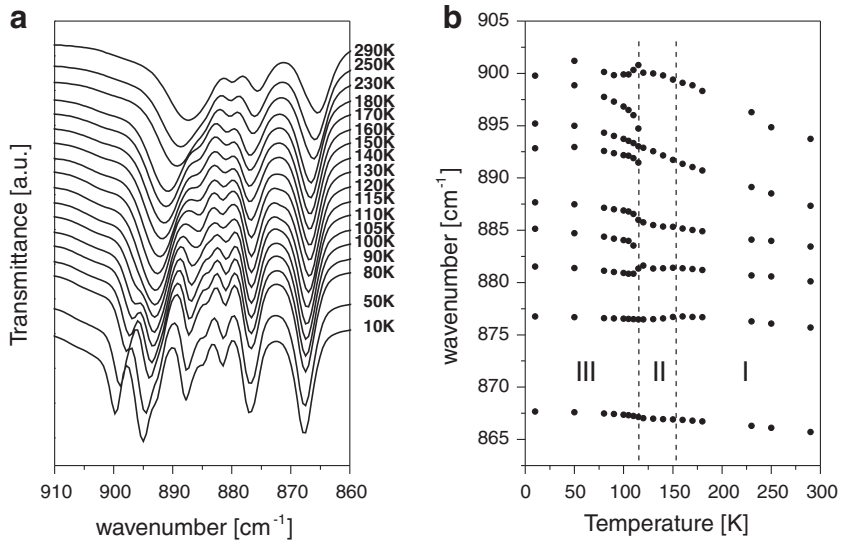

Fig. 5. (a) Temperature evolution of the IR spectra in the $\nu(CH_2)$ vibration region (910–860 cm^{-1}) and (b) temperature dependence of the wavenumber positions of the $\nu(CH_2)$ modes.

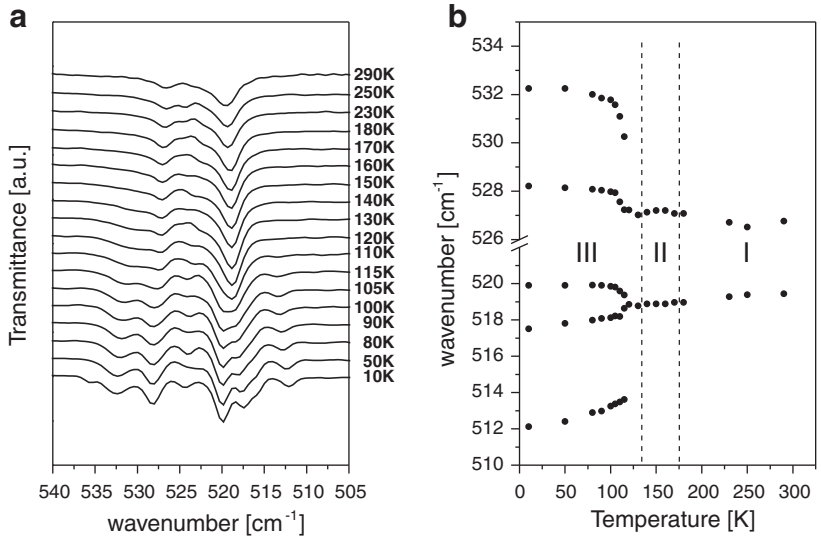

Fig. 6. (a) Temperature evolution of the IR spectra in the $\nu_4(BF_4)$ vibration region (540–505 cm^{-1}) and (b) temperature dependence of the wavenumber positions of these modes.

in Fig. 2. Fig. 3 shows infrared and Raman spectra of deuterated $[ND_2(C_2H_4)_2O][BF_4]$ at room temperature. The IR spectra in a frequency range 3000–2800, 1500–1350, 750–700 cm^{-1} are shown as a dotted line as Nujol bands appear in these regions. To cover these regions we measured infrared spectra of $[NH_2(C_2H_4)_2O][BF_4]$ (normal and deuterated) in Fluorolube mulls, however, only at 300 K. The experimental and calculated frequencies of $[NH_2(C_2H_4)_2O][BF_4]$ bands and experimental frequencies of the deuterated homologue are collected in Supplementary Table S1. The selected data related to wavenumber regions analyzed below are shown in Table 4.

An analysis of the isolated bands arising from some internal vibrations (for instance the band at 769 cm^{-1} in IR and Raman spectra arising from $\nu_1(BF_4)$) clearly shows lack of the correlation field (or Davydov) splitting in powder spectra of the title crystal. Therefore, in the discussion of the internal vibrations it is enough to take into account only the site approach for each ion. In the case of the tetrafluoroborate ions it is clearly seen that the anion symmetry is not tetrahedral (T_d; as it was suggested by Szklarz et al. [16]) but either C_s or C_1. One should mention that on the basis of vibrational spectra measured for the powder sample these two cases are impossible to distinguish.

Tentative assignments of the observed bands arising from cationic vibrations are based on a comparison with a morpholine IR spectrum [27] and similar heterocyclic compounds [28–31]. The work of Bates et al. [32] and [26] were used to assign the $[BF_4]^-$ anion vibrations. The assignments of the (NH_2^+) group were made taking into account results reported for protonated secondary amines [33].

From data in Table 4 it clearly follows that the assignments of $[BF_4]^-$ vibration bands and most of the cationic modes are well consistent with the calculated frequency values. The most significant divergences are seen in a case of (NH_2^+) and ν(C–N) modes. ν(C–N) stretching vibrations, in comparison with the calculated values, are shifted towards high frequencies. To assign correctly modes corresponding to (NH_2^+) vibrations, IR and Raman spectra of deuterated $[ND_2(C_2H_4)_2O][BF_4]$ were used. The protonated amine group is involved in one N–H(1D)···O(1) and at least two various N–H···F hydrogen bonds: (N1–H(1C)···F(6) and N(1)–H(1C)···F(3) or N1–H(1C)···F(6)^a and N(1)–H(1C)···F(3)^a, respectively (Table 4 in [16]), which causes a shifting of the stretching vibration bands towards low frequencies. Rocking, wagging, twisting and scissoring vibration bands of the (NH_2^+) group occur in regions characteristic of other protonated secondary amines. From Fig. 3 one can see that for deuterated $[ND_2(C_2H_4)_2O][BF_4]$ in a wavenumber region 3300–3000 cm^{-1} almost all bands of (NH_2^+) modes disappear and the other ones emerge in 2500–2100 cm^{-1} region. The deuterium substitution causes frequency shift by a factor of 1.37, which is almost equal to $\sqrt{2}$ of the isotopic shift. The same situation occur in a case of other (ND_2^+) modes.

An analysis of the evolution of IR spectra performed in a wavenumber region between 3300–3000 cm^{-1} assigned mainly to the stretching vibrations N–H···O and N–H···F (Fig. 4) shows that some components change their positions or split into several components at temperature close to T_c = 117 K. It should be noted that mentioned above changes are more significant at the low temperature phase transition than at the other one. The modes at 3028 and 3082 cm^{-1} are bands the most sensitive to the **II** → **III** phase transition. On cooling these bands split into some components just below 117 K. In a case of the band at 3237 cm^{-1} the splitting has occurred below **I** → **II** phase transition.

Fig. 5 presents an evolution of IR spectra and temperature dependence of the positions of the bands in a region assigned to $\nu(CH_2)$ vibrations (910–860 cm^{-1}). At low temperature eight bands can be assigned to $\nu(CH_2)$ vibrations and one band to C–C (at 868 cm^{-1}) vibration. Again, the remarkable changes in positions of the bands are observed at *ca.* 117 K. Some bands appear just below T_c (bands at 895, 893 cm^{-1}), whereas the band at 880 cm^{-1} splits into two components. The characteristic feature of the temperature behavior of some bands (e.g. 888 and 895 cm^{-1} at 300 K) is a relatively large temperature coefficient of the change in their positions. However, no discontinuity in the temperature dependence of their positions is observed at 153 K (**I** → **II** PT).

Fig. 6 shows an evolution of IR spectra *vs* temperature in a wavenumber region between 540–505 cm^{-1}. The bands in this wavenumber range arise from ν_4 vibrations of the $[BF_4]^-$ anions (see Table 4). At the phase transition temperature (transition to the phase **III**) the band at 527 cm^{-1} shifts towards high wavenumbers (528 cm^{-1}), whereas the band at 519 cm^{-1} splits into two components (517 and 520 cm^{-1}). Moreover, two new bands appear over the phase **III** at 532 and 512 cm^{-1}.

The appearance of the significant changes in IR spectra on changing temperature in wavenumber ranges corresponding to the vibrations of the (NH_2^+) groups as well as of the $[BF_4]^-$ anions

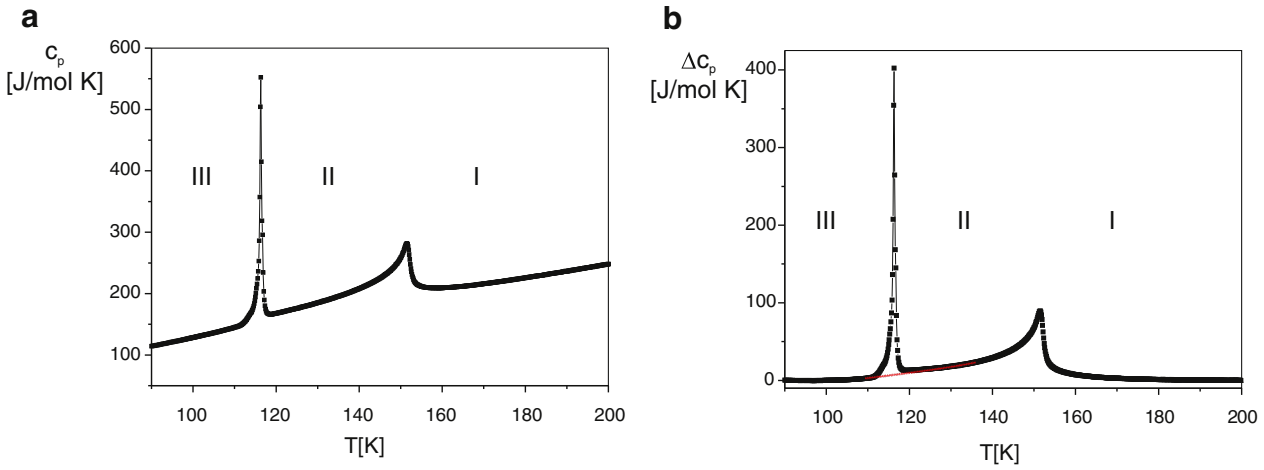

Fig. 7. Temperature dependence of the specific heat of $[NH_2(C_2H_4)_2O][BF_4]$ compound (a) and excess specific heat (b). The red line (in part (b)) gives a provisional separation of two transitions. (For interpretation of the references to colour in this figure legend, the reader is referred to the web version of this article.)

confirms the supposition that the anions and N–H···Y hydrogen bonds formed by them play a crucial role in the mechanism of the phase transitions in the $[NH_2(C_2H_4)_2O][BF_4]$ crystal.

6. Thermodynamic properties

Fig. 7a shows temperature dependence of the specific heat during cooling in a limited temperature range. Two anomalies connected with the previously mentioned phase transitions were detected at temperatures 117 K and 153 K. The AC calorimeter can be used only for qualitative studies of first-order transitions. Nevertheless, we were able to estimate a very small temperature hysteresis, of the order of 0.322 K, for the "lock-in" first-order transition at 117 K. It should be taken into account that absolute values of the specific heat could be determined in relation to a reference, which in our case was a sapphire sample. The anomalous specific heat excess Δc_p was determined by a subtraction of a lattice background approximated by a polynomial. It is rather difficult to split the $\Delta c_p(T)$ run into two parts corresponding to two phase transitions. In order to get more reliable heat flow values, the data related to the incommensurate phase (IC) and to the **I** → **II** transition were fitted using an exponential function extrapolated to the background line (see Fig. 7b).

Thermal parameters for the second-order transition (153 K) to the IC phase were estimated: an excess entropy $\Delta S \approx 7.13$ J/mol · K, and an excess enthalpy $\Delta H = 983.4$ J/mol. The values obtained are quite high as for the N-IC transition (e.g. the ΔS value is comparable with the value reported for crystals of the A_2BX_4-type with tetramethylammonium cations [34]). The critical behavior of the c_p-anomaly at this transition has been analyzed with the preasymptotic 3D XY model renormalization group expression given by Bagnuls and Bervillier, [35]:

$$\Delta c_p = A^{\pm}|t|^{-\alpha}(1 + D_1^{\pm}|t|^{\Delta_1} + D_2^{\pm}|t|) + B_{cr} \quad (1)$$

where superscripts ± denote parameter values for temperature above and below the transition point, T_i; $t = (T - T_i)/T_i$ is a reduced temperature; $A^{\pm}$ is a critical amplitude; α-a critical exponent; $D_1^{\pm}$ and $D_2^{\pm}$ are the first and second-order correction terms; B_{cr}-a critical constant; and Δ_1 is a subcritical exponent.

In Fig. 8a the anomaly of the heat capacity $\Delta c_p/R$ at the normal-incommensurate transition (circles) and the 3D XY fit (solid line) are shown. The procedure of fitting, similar to that used by Haga et al. [36], was applied. The exponent $\alpha = -0.007$, the critical amplitude ratio $A^-/A^+ = 0.869$, $D_1^+ = -0.045$, $D_1^- = -0.041$, $\Delta_1 = 0.524$, $D_2^{\pm} = -0.002$ and a dimensionless factor: $R_B^+ = A^+|D_1^+|^{\frac{\alpha}{\Delta_1}} B_{cr}^{-1} \approx -0.944$ are quite close to the theoretically expected for 3D XY model. For points above T_i a slight discrepancy between fitting

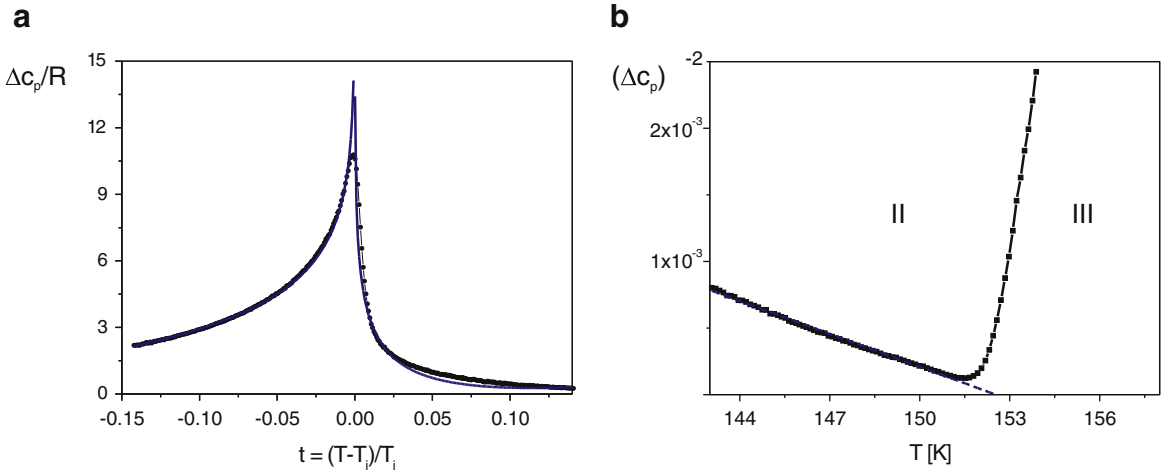

Fig. 8. (a) Excess specific heat $\Delta c_p/R$ near the normal-incommensurate transition (filled circles) and fit with the Eq. (1) (solid line) and (b) temperature dependence of $(\Delta c_p)^{-2}$. The metastable limit is also shown.

and experimental points can be noted. It should be also pointed that the transition is not far (ΔT = 0.65 K) from the tricritical point (Fig. 8b).

7. Proton magnetic resonance (^{1}H NMR) studies

The temperature dependence of the spin–lattice relaxation time may be divided into three parts separated by two phase transition temperatures, 117 K and 153 K (Fig. 9). Below 117 K two well separated minima of T_1 relaxation time are observed with comparable depths: 0.24 and 0.27 s at 94 K and 111 K, respectively. In the temperature range 117–153 K (IC phase) a slope of the curve found seems to be unexpectedly lower than that detected at low temperature. Above 153 K (1000/T < 6.5 K^{-1}) only the left side of the minimum of T_1 relaxation time is reached with nearly the same slope as for the other minimum found at low temperature. It should be emphasized that both phase transitions are not accompanied by any sudden discontinuities/jumps in the T_1 value-its temperature dependence reveals only slightly different slopes in particular temperature ranges.

It is obvious that below 117 K (1000/T > 8.5 K^{-1}) two different nonequivalent relaxation processes exist: one proton of the (NH_2^+) group is moving along the hydrogen bond of N–H···O type, whereas the other one along N–H···F bond. It was assumed that dynamics of both corresponding protons in three nonequivalent cations and protons involved in the two types of hydrogen bonds is comparable. Contributions of the two protons to the relaxation phenomena are equal, which may be deduced from almost the same depths of both minima on the dependence of T_1 versus reciprocal temperature. It means that the general formula for the reciprocal value of T_1 should be written as:

$$\frac{1}{T_1} = \frac{N_O}{N}\frac{1}{T_{1O}} + \frac{N_F}{N}\frac{1}{T_{1F}} \tag{2}$$

where T_{1O} and T_{1F} denote the relaxation times of the protons in N–H···O and N–H···F hydrogen bridges, respectively; N_O and N_F denote the numbers of the relaxing protons of morpholinium cations participating in hydrogen bonds, and N denotes the total number of protons in morpholinium cations in the unit cell (Z = 12). In our case N_i/N = 12/120. The temperature dependence of the spin–lattice relaxation time T_{1i} was analyzed by a BPP theory, using an equation:

$$\frac{1}{T_{1i}} = C\left[\frac{\tau_c}{1+\omega^2\tau_c^2} + \frac{4\tau_c}{1+4\omega^2\tau_c^2}\right] \tag{3}$$

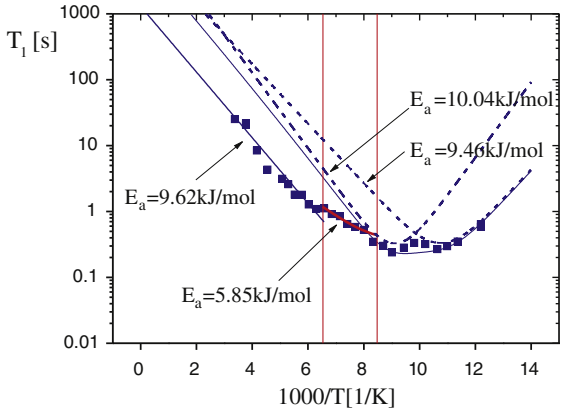

Fig. 9. The temperature dependence of the spin–lattice relaxation time (^{1}H NMR) of $[NH_2(C_2H_4)_2O][BF_4]$. Solid lines are results of theoretical fitting and dashed lines denote the both components according to Eq. (2).

In this equation ω represents a resonance angular frequency, C-relaxation constant and τ_c is a correlation time. The temperature dependence of the correlation time is described by the Arrhenius law: $\tau_c = \tau_0 exp(E_a/RT)$, where τ_0 is a correlation time at the limit infinite temperature, E_a-the height of the barrier, R-gas constant. This gives three sets of parameters for the three temperature regions of T_1 analyzed. The values of E_a and τ_0 estimated using Eqs. (2) and (3) are shown in Table 5. The data relate to two assumed relaxation processes of the (NH_2^+) protons in the morpholinium cation. The activation energy values, evaluated for the high temperature regions of $T_1(1000/T)$, are collected in Table 5 as well.

It should be noted that the estimated activation energy values at high temperature (above 153 K, 9.62 kJ/mol) are very close to that found at low temperature (below 117 K, 10.04 and 9.46 kJ/mol). It may be explained by the fact that mechanism of both phase transitions, at 117 and at 153 K, is assigned to the changes in molecular dynamics of anions, which seems to affect insignificantly the cationic internal motions.

8. Discussion

Our previous X-ray investigations on a single crystal of $[NH_2(C_2H_4)_2O][BF_4]$, carried out at several temperatures, suggested that thermodynamical properties and the phase situation was related to a disorder of the $[BF_4]^-$ groups [16]. Scanning calorimetry (DSC) measurements allowed us, besides an establishment of a sequence of phase transitions, to roughly determine energetic effects (entropic) for the I-st order phase transition, **II** → **III**, at about 117 K. The dielectric studies indicated, moreover, a step-wise freezing of some dipolar group motions at this temperature. Except these aspects the molecular mechanism of both phase transitions was unclear. It concerns mainly the **I** → **II** transition of continuous nature at 153 K. By definition this transition could not be analyzed in details only on the basis of DSC results. Thus, the AC calorimetric results, presented in this work, allow us to analyze more deeply this mechanism as well as to give a thermodynamical characteristics of this continuous transition. The estimated excess entropy for this transition amounts to about $\Delta S \approx 7.13$ J/mol · K, which indicates a clear "order–disorder" mechanism of the **I** → **II** PT. The magnitudes of ΔS_{tr} for the low temperature transition obtained from either DSC or AC calorimetric measurements were comparable, being of about 3.5–4.5 J/mol · K. Taking into account the four-site model of the $[BF_4]^-$ group disorder in the phase **I**, proposed on the basis of the X-ray data, the total value of ΔS_{tr} should equal to ΔS_{tr}(**I** → **II**) + ΔS_{tr}(**II** → **III**), which gives approx. ≈10.6–11.6 J/mol · K. This value agrees well with the theoretical one for the four-site model ($Rln4 \approx 11.52$ J/mol · K). This result indicates univocally that the dynamics of the $[BF_4]^-$ groups is mainly responsible for the phase transition mechanism at 153 K. This PT is probably accompanied by a significant retardation of the $[BF_4]^-$ anion reorientational motion, whereas at 117 K this motion is completely locked.

Proton magnetic resonance studies revealed an unexpected picture of the possible molecular dynamics, particularly in the low temperature phase (T < 117 K). If we took into account only

Table 5
Parameters characterizing detected proton relaxation calculated from the fit of Eq. (3) to $T_1(T)$ experimental points below 117 K and the activation energies.

	<117 K	117–153 K	>153 K
E_a [kJ/mol]	10.04 9.46	5.85	9.62
τ_0 [s]	$0.8 \cdot 10^{-13}$ $1.5 \cdot 10^{-14}$	–	–
C [s^{-2}]	$3.16 \cdot 10^9$	–	–

crystallographic results this picture should be different. The X-ray results indicated that the morpholinium cations were rather rigid in the crystal structure, being involved in the one-dimensional chain formed via N–H···O hydrogen bonds. These chains were additionally stabilized by N–H···F hydrogen bonds to the $[BF_4]^-$ anions. Thus, we could expect rather weak temperature dependence of T_1 relaxation time. An appearance of two minima on T_1 *vs.* temperature curve at low temperature proved that we dealt with some proton dynamics in the phase **III**. There is no doubt that merely the proton dynamics of the (NH_2^+) groups, which are engaged in the medium strong hydrogen bonds, could contribute to the relaxation processes as the cation and anion motions are already frozen. These relaxation processes are indicated by the presence of two low temperature minima in the phase **III**. The lack of temperature anomalies of T_1 value around the phase transitions at 153 and 117 K additionally confirms that the morpholinium cations are inactive in the mechanism of the structural phase transitions. In this context the character of the dielectric response is not fully understandable (see Fig. 7 in [16]). The dielectric response reveals a relatively high change of the dielectric increment: $\Delta\varepsilon' \approx 4.5$ at 117 K. If we do not relate it to the dynamics of the polar morpholinium cations, a change of the proton dynamics in hydrogen bonds, which is correlated with the $[BF_4]^-$ motions, seems to be responsible for a change in a dipole moment of the unit cell. As a consequence we should observe a jump in the dielectric increment when the $[BF_4]^-$ motion is frozen. It should be emphasized that no dielectric relaxation process has been found over the phase **II** up to 2 MHz. It means that the motion of the $[BF_4]^-$ anions is expected to be rather fast, thus dielectric relaxation has to be shifted up to the microwave or submillimeter frequency region. On the other hand, when a motion of the hydrogen in N–H···F hydrogen bonds is taken into account, we suppose that it should be relatively slow and could be observed in infrared spectra on approaching the PT at 119 K. This proton motion should be coupled with the reorientations of the $[BF_4]^-$ anions as it had been already concluded in [16]. This type of vibrations is revealed as IR phonon anomalies for distorted phases even in non-ferroelectric crystals [37]. Far infrared measurements for the single crystal of $[NH_2(C_2H_4)_2O][BF_4]$ are planned.

Studies on the vibrational properties in a wide temperature range were supposed to throw more light on a role of both cation and anion dynamics as regards to the mechanism of the phase transitions at the molecular level. Substantial changes in IR spectra were found near both the **I** → **II** and **II** → **III** PTs in $[NH_2(C_2H_4)_2O][BF_4]$ in wavenumber ranges corresponding to the stretching vibrations of the (NH_2^+) groups as well as to the $[BF_4]^-$ vibrations. This observation confirms a crucial role of the hydrogen bond dynamics as well as the anionic reorientational motion in the mechanism of these phase transitions.

9. Conclusions

1. Significant changes with temperature in the IR spectrum, close to 117 and 153 K, indicate that (NH_2^+) and $[BF_4]^-$ groups contribute simultaneously to the phase transitions mechanism. (NH_2^+) and C–C stretching as well as the $\nu_4(BF_4)$ modes appear to be the most sensitive to the phase transitions.
2. The AC calorimetric studies allow us to evaluate precisely thermodynamic parameters of the normal-incommensurate type phase transition at 153 K. This transition may be classified as the pure "order–disorder" type ($\Delta S_{tr} \approx 7.1$ J/mol K) and is governed by the reorientational motion of the $[BF_4]^-$ groups. The transition is close to the tricritical point.
3. The relaxation processes, observed in ^{1}H NMR studies, may be explained in terms of the proton dynamics in N–H···O and N–H···F hydrogen bonds. They are believed to play a crucial role in the phase transition mechanism at 117 and 153 K.

Acknowledgments

The calculations were performed on computers of Wroclaw Center for Networking and Supercomputing, calculating Grant No. 2006/5, and in Interdisciplinary Center for Mathematical and Computational Modeling, Warsaw University, calculating Grant No. G30-15. MATERIALS STUDIO package was used under POLAND COUNTRY–WIDE LICENSE. This work was partially supported by ZIBJ Dubna contract No. 04-4-1069-2009/2010.04.29.

Appendix A. Supplementary data

Supplementary data associated with this article can be found, in the online version, at doi:10.1016/j.chemphys.2011.01.002.

References

[1] G.R. Desiraju, Crystal Engineering: The Design of Organic Solids, Elsevier Scientific Publishers, Amsterdam and New York, 1989.
[2] J.-L. Lehn, Supramolecular Chemistry: Concepts and Perspectives, VCH, New York, 1995.
[3] G. Xu, G.-G. Guo, M.-S. Wang, Z.-J. Zhang, W.-T. Chen, J.-S. Huang, Angew. Chem. Int. Ed. 46 (2007) 3249.
[4] Q. Ye, D.-W. Fu, H. Tian, R.-G. Xiong, P.W.H. Chan, S.D. Huang, Inorg. Chem. 47 (3) (2008) 772.
[5] D.-W. Fu, W. Zhang, R.-G. Xiong, Cryst. Growth Des. 8 (9) (2008) 3461.
[6] H. Ratajczak, J. Baran, J. Barycki, S. Debrus, M. May, A. Pietraszko, H.M. Ratajczak, A. Tramer, J. Venturini, Mol. Struct. 555 (2000) 149.
[7] C.-Y. Chen, Z.-B. Wei, Z.-H. Zhoua, S.W. Ng, Acta Cryst. E59 (2003) o1030.
[8] I. Majerz, T. Głowiak, A. Koll; J. Mol. Struct. 374 (1996) 339.
[9] H. Ishida, B. Rahman, S. Kashino, Acta Cryst. C57 (2001) 1450.
[10] H. Shodel, W. Seitz, H. Bock, J.W. Bats, Monatsh. Chem. 127 (1996) 63.
[11] G.S. Bahra, P.A. Chalonerb, L.M. Dutta, W. Healy, P.B. Hitchcock, Journal of Crystal Growth 225 (2001).
[12] K. Lava, K. Binnemans, T. Cardinaels, J. Phys. Chem. B 113 (2009) 9506.
[13] C.-X. Yin, F.-J. Huo, P. Yang, Acta Cryst. E62 (2006) o2084.
[14] M.S. Grigoriev, K.E. German, A.Ya. Maruk, Acta Cryst. E64 (2008) o390.
[15] M.S. Grigoriev, K.E. German, A.Ya. Maruk, Acta Cryst. E63 (2007) m2355.
[16] P. Szklarz, M. Owczarek, G. Bator, T. Lis, K. Gatner, R. Jakubas, J. Molec. Struc. 929 (2009) 48.
[17] M. Owczarek, P. Szklarz, R. Jakubas, T. Lis, Acta Cryst. E64 (2008) o667.
[18] J. Petzelt, Phase Trans. 2 (1981) 155.
[19] B.A. Strukov, A.P. Levanyuk, Ferroelectric Phenomena in Crystals, first ed., Springer-Verlag, Berlin Heidelberg, 1998. p. 227.
[20] B. Delley, J. Chem. Phys. 92 (1990) 508.
[21] B. Delley, J. Chem. Phys. 113 (2000) 7756.
[22] http://www.accelrys.com
[23] A.D. Becke, J. Chem. Phys. 88 (1988) 2547.
[24] C. Lee, W. Yang, R.G. Parr, Phys. Rev. B 37 (1988) 786.
[25] P. Pulay, G. Fergasi, F. Pang, J.E. Boggs, J. Am. Chem. Soc. 101 (1979) 2550.
[26] A. Muller, B. Krebs, J. Mol. Spectrosc. 24 (1967) 180.
[27] D. Vedal, O.H. Ellestad, P. Klaboe, Spectrochim. Acta 32A (1976) 877.
[28] O.H. Ellestad, P. Klaboe, Spectrochim. Acta 29A (1973) 1247.
[29] D. Vedal, O.H. Ellestad, P. Klaboe, Spectrochim. Acta 31A (1975) 339.
[30] D. Vedal, O.H. Ellestad, P. Klaboe, Spectrochim. Acta 31A (1975) 355.
[31] O.H. Ellestad, P. Klaboe, Spectrochim. Acta 27A (1971) 1025.
[32] J.B. Bates, A.S. Quist, Spectrochim. Acta 31A (1975) 1317.
[33] D. Cook, Can. J. Chem. 42 (1964) 2292.
[34] H.Z. Cummins, Phys. Rep. 185 (1990) 211.
[35] C. Bagnuls, C. Bervillier, Phys. Rev. B32 (1985) 7209.
[36] H. Haga, A. Onodera, Y. Shiozaki, K. Ema, H. Sakata, J. Phys. Soc. Japan. 64 (3) (1995) 822.
[37] J. Petzelt, Phys. Lett. A 48 (1974) 341.